Journal of Molecular Structure 1002 (2011) 10–18

Contents lists available at ScienceDirect

Journal of Molecular Structure

journal homepage: www.elsevier.com/locate/molstruc

X-ray structures and computational studies of several cathinones

Jacek E. Nycz [a,*], Grzegorz Malecki [a], Marcin Zawiazalec [b], Tadeusz Pazdziorek [b]

[a] Institute of Chemistry, University of Silesia, ul. Szkolna 9, PL-40007 Katowice, Poland
[b] Department of Chemistry, Forensic Laboratory, The Regional Headquarters, Katowice, Poland

ARTICLE INFO

Article history:
Received 16 May 2011
Received in revised form 22 June 2011
Accepted 23 June 2011
Available online 6 July 2011

Keywords:
Cathinone
4-MEC
Methylone
Mephedrone
Buphedrone
X-ray

ABSTRACT

2-(Ethylamino)-1-(4-methylphenyl)propan-1-one (shortly named 4-MEC) (**1a**), 1-(1,3-benzodioxol-5-yl)-2-(methylamino)propan-1-one (shortly named methylone or 3,4-methylenedioxymethcathinone) (**1b**), 1-(3,4-dimethylphenyl)-2-(methylamino)propan-1-one (**1c**), 2-methylamino-1-(4-methylphenyl)propan-1-one (shortly named mephedrone; 4-MMC or 4-methylmethcathinone) (**1d**) and 2-(methylamino)-1-phenylbutan-1-one (shortly named buphedrone) (**1e**) and their aminium salts (**2a–e**), are examples of cathinones which were characterized by FTIR, UV–Vis, multinuclear NMR spectroscopy. By single crystal X-ray diffraction method structures of **2a**, **2b**, **2c** and **2d** were determined. NMR solution spectra showed readily diagnostic H-1 and C-13 signals from methyl, ethyl, *N*-methyl or *N*-ethyl groups. The diastereotopic methylene protons of **1a** appear as an ABX_3, and **1e** and **2e** appear as an $ABMX_3$ system. The geometries of the studied compounds were optimized in singlet states using the density functional theory (DFT) method with B3LYP functional. Electronic spectra were calculated by TDDFT method. In general, the predicted bond lengths and angles are in good agreement with the values based on the X-ray crystal structure data.

1. Introduction

The cathinones are a class of compounds containing α-aminopropiophenone moiety. They are derivatives of cathinone, a natural amphetamine-like alkaloid, which is the major pharmacologically active constituent extracted from fresh leaves and stems of *Catha edulis* Forsk, Celastraceae (Khat) [1]. This shrub is usually found in the southwestern part of the Arabian Penisula and East Africa, where it has been used for centuries for both spiritual and recreational purposes. Khat has been recorded in literature for the purpose of alleviating depression as early as 1237 by physician Nagub Ad Din [2,3].

There are a number of synthetic cathinones that are used recreationally. They are expected to act as a central nervous system stimulants by promoting the release of monoamine neurotransmitters and likely inhibiting their reuptake [4]. The first described synthesis of mephedrone as an example of cathinone was in 1929 [5]. Mitochondrial monoamine oxidases are flavin-containing enzymes (FAD or FMN) to catalyze the oxidative deamination of neurotransmitters and exogenous arylalkylamines [6]. The postulated metabolic pathways of cathinones are through the *N*-dealkylation and demethylenation, followed by the *O*-methylation and reduction of the keto moiety to alcohols, and the oxidation of the tolyl moiety to the corresponding alcohols or carboxylic acids [7,8].

Recently we presented two compounds, 1-pentyl-3-(4-methoxy-1-naphthoyl)indole (shortly named JWH-081) and 2-(2-methoxy-phenyl)-1-(1-pentyl-1*H*-indol-3-yl)-ethanone (shortly named JWH-250), as examples of cannabinoids. They were characterized by FTIR, UV–Vis, multinuclear NMR spectroscopy and single crystal X-ray diffraction method [9].

The current work focuses on further computational and X-ray studies to ascertain the atomic charges of selected cathinones, the energy of the frontier orbitals and the conformation of groups, which have not been determined by crystallographic studies yet. The identification of cathinones are of medical and forensic or doping interest.

2. Experimental

2.1. General

NMR spectra were obtained with Bruker Avance 400 operating at 400.13 MHz (^{1}H) and 100.5 MHz (^{13}C) at 21 °C; chemical shifts referenced to ext. TMS (^{1}H, ^{13}C); coupling constants are given in Hz. The ^{1}H and ^{13}C NMR calculations were performed with the ACD Labs NMR Predictor v.7 program considering the influence of different solvents ($CDCl_3$ or DMSO). FTIR spectra were recorded on a Perkin Elmer spectrophotometer in the spectral range 4000–450 cm^{-1} with the samples in the form of KBr pellets. Electronic spectra were measured on a spectrophotometer Lab. Alliance UV–Vis 8500 in the range 500–180 nm in CH_2Cl_2 solution. Chromatography was

* Corresponding author. Tel.: +48 323591206; fax: +48 322599978.
E-mail address: jnycz@us.edu.pl (J.E. Nycz).

0022-2860/$ - see front matter © 2011 Elsevier B.V. All rights reserved.
doi:10.1016/j.molstruc.2011.06.030

carried out on Silica Gel 60 (0.15–0.3 mm) Machery Nagel. Melting points were determined on MPA100 OptiMelt melting point apparatus and uncorrected. Compounds **2a**, **2b**, **2c**, **2d** and **2e** were purchased from LGC Standards.

2.1.1. Synthesis of 1a, 1b, 1c, 1d and 1e

The water solution of **2a**, **2b**, **2c**, **2d** or **2e** was alkalified by K_2CO_3. Reagents were shaken for a few minutes. The mixture was poured into CH_2Cl_2. The organic phase was separated and dried by $MgSO_4$. After the solvent was evaporated, the residue was purified by chromatography.

2.1.2. Crystallization of 2a, 2b, 2c, 2d and 2e

The colorless crystals suitable for X-ray analysis were obtained by slowly solvents' evaporating at room temperature for **2a** and **2b**, and in −35 °C for **2c** and **2d**. Crystallization of **2e** is in progress.

2-(Ethylamino)-1-(4-methylphenyl)propan-1-one (**1a**) (yellowish liquid) ^{1}H NMR ($CDCl_3$) δ = 1.10 (t, J_{HH} = 7.1 Hz, 3H, CH_2CH_3), 1.29 (d, J_{HH} = 7.0 Hz, 3H, $CHCH_3$), 2.22 (m, 1H, NH), 2.41 (s, 3H, 4-CH_3Ar), 2.56 (ABX_3, J_{HHgem} = 12.8 Hz, J_{HH} = 7.1 Hz, 2H, CH_2CH_3), 4.29 (q, J_{HH} = 7.0 Hz, 1H, $CHCH_3$), 7.27 (d, J_{HH} = 8.2 Hz, 2H, aromatic), 7.86 (d, J_{HH} = 8.2 Hz, 2H, aromatic); ^{13}C{^{1}H} NMR ($CDCl_3$) δ = 15.44, 20.07, 21.63, 42.35, 57.51, 128.33, 129.42, 133.10, 144.21, 203.22.

N-Ethyl-1-(4-methylphenyl)-1-oxopropan-2-aminium chloridum (**2a**) (colorless solid) m.p. = 198–199 °C (methanol); ^{1}H NMR ($CDCl_3$) δ = 1.53 (t, J_{HH} = 7.3 Hz, 3H, CH_2CH_3), 1.81 (d, J_{HH} = 7.2 Hz, 3H, $CHCH_3$), 2.43 (s, 3H, 4-CH_3Ar), 3.06–3.27 (m, 2H, CH_2CH_3), 4.96–5.06 (m, 1H, $CHCH_3$), 7.31 (d, J_{HH} = 8.0 Hz, 2H, aromatic), 7.86 (d, J_{HH} = 8.2 Hz, 2H, aromatic), 9.02 (m, 1H, NH_2), 10.69 (m, 1H, NH_2); ^{13}C{^{1}H} NMR ($CDCl_3$) δ = 11.79, 16.86, 21.80, 42.12, 57.83, 128.96, 129.89, 130.44, 146.05, 194.25; IR (KBr): 3438 (νNH), 2946 (νPhH), 2819, 2765 (νCH_3), 1651 (νC = O, scissor. NH_2), 1602 (νC=C), 1459 (νPhH), 1340, 1263 (νC-N), 768, 743 (wag. NH_2); UV–Vis (methanol; [nm]) (log ε): 259.0 (5.17), 211.0 (5.01); X-ray CCDC 823158.

1-(1,3-Benzodioxol-5-yl)-2-(methylamino)propan-1-one (**1b**) (yellowish liquid). ^{1}H NMR ($CDCl_3$) δ = 1.21 (d, J_{HH} = 7.0 Hz, 3H, $CHCH_3$), 2.27 (bs, 3H, NCH_3), 4.05 (q, J_{HH} = 7.0 Hz, 1H, $CHCH_3$), 5.97 (s, 2H, OCH_2), 6.79 (d, J_{HH} = 8.2 Hz, 1H, aromatic), 7.38 (s, 1H, aromatic), 7.51 (d, J_{HH} = 8.2 Hz, 1H, aromatic); ^{13}C{^{1}H} NMR ($CDCl_3$) δ = 19.79, 34.50, 59.15, 101.78, 107.90, 107.92, 124.32, 130.36, 148.22, 151.88, 201.24.

1-(1,3-Benzodioxol-5-yl)-*N*-methyl-1-oxopropan-2-aminium chloridum (**2b**) (colorless solid) m.p. = 225–226 °C (methanol); ^{1}H NMR ($CDCl_3$) δ = 1.80 (d, J_{HH} = 7.2 Hz, 3H, $CHCH_3$), 2.80 (bs, 3H, NCH_3), 4.76 (bs, 1H, $CHCH_3$), 6.11 (s, 2H, OCH_2), 6.92 (d, J_{HH} = 8.3 Hz, 1H, aromatic), 7.42 (s, 1H, aromatic), 7.53 (d, J_{HH} = 8.8 Hz, 1H, aromatic); ^{13}C{^{1}H} NMR (DMSO-*d6*) δ = 25.26, 40.13, 67.44, 111.99, 117.42, 118.04, 135.32, 136.97, 157.71, 162.18, 203.81; IR (KBr): 3435 (νNH), 2920 (νPhH), 2799, 2735 (νCH_3), 1679 (νC=O + scissor. NH_2), 1603 (νC=C), 1502, 1452 (νPhH), 1349, 1299 (νC-N), 1261, 1090 (νC-O), 767, 741 (wag. NH_2); UV–Vis (methanol; [nm]) (logε): 307.8 (4.97), 270.2 (4.88), 224.8 (5.19), 192.6 (5.41); X-ray CCDC 819333.

1-(3,4-Dimethylphenyl)-2-(methylamino)propan-1-one (**1c**) (yellowish liquid) ^{1}H NMR ($CDCl_3$) δ = 1.19 (d, J_{HH} = 7.1 Hz, 3H, CH_3CH), 1.93 (s, 1H, NH), 2.21 (s, 3H, 3-CH_3Ar), 2.22 (s, 3H, 4-CH_3Ar), 2.26 (s, 3H, NCH_3), 4.10 (q, J_{HH} = 7.0 Hz, 1H, CH_3CH), 7.12 (d, J_{HH} = 7.9 Hz, 1H, aromatic), 7.61 (dd, J_{HH} = 7.9 Hz, J_{HH} = 1.6 Hz, 1H, aromatic), 7.66 (s, 1H, aromatic); ^{13}C{^{1}H} NMR ($CDCl_3$) δ = 19.47, 19.58, 19.70, 34.40, 59.05, 125.65, 129.03, 129.65, 133.40, 136.82, 142.58, 202.85.

1-(3,4-Dimethylphenyl)-*N*-methyl-1-oxopropan-2-aminium chloridum (**2c**) (colorless solid) m.p. = 211–212 °C (methanol); ^{1}H NMR ($CDCl_3$) δ = 1.78 (d, J_{HH} = 7.2 Hz, 3H, CH_3CH), 2.30 (s, 3H, 3-CH_3Ar), 2.32 (s, 3H, 4-CH_3Ar), 2.84 (s, 3H, NCH_3), 4.95 (q, J_{HH} = 7.3 Hz, 1H, CH_3CH), 7.24 (d, J_{HH} = 8.2 Hz, 1H, aromatic), 7.67 (dd, J_{HH} = 7.9 Hz, J_{HH} = 1.4 Hz, 1H, aromatic), 7.72 (s, 1H, aromatic), 9.92 (bs, 1H, NH_2); ^{13}C{^{1}H} NMR ($CDCl_3$) δ = 16.48, 19.77, 20.21, 31.64, 59.25, 126.54, 129.88, 130.32, 130.78, 137.71, 144.74, 194.43; IR (KBr): 3363 (νNH), 2907 (νPhH), 2806, 2735 (νCH_3), 1688 (νC=O), 1675 (scissor. NH_2), 1605, 1572 (νC=C), 1464 (νPhH), 1399, 1250 (νC-N), 763, 730 (wag. NH_2); UV–Vis (methanol; [nm]) (log ε): 262.0 (5.32), 210.0 (5.33); X-ray CCDC 822797.

2-Methylamino-1-(4-methylphenyl)propan-1-one (**1d**) (yellowish liquid) ^{1}H NMR ($CDCl_3$) δ = 1.23 (d, J_{HH} = 7.1 Hz, 3H, $CHCH_3$), 2.26 (bs, 1H, NH), 2.30 (s, 3H, 4-CH_3Ar), 2.34 (s, 3H, NCH_3), 4.14 (q, J_{HH} = 7.0 Hz, 1H, CH), 7.21 (d, J_{HH} = 8.1 Hz, 2H, aromatic), 7.80 (d, J_{HH} = 8.2 Hz, 2H, aromatic); ^{13}C{^{1}H} NMR ($CDCl_3$) δ = 19.64, 21.55, 34.47, 59.21, 128.25, 129.35, 133.01, 144.17, 202.68.

1-(4-Methylphenyl)-*N*-methyl-1-oxopropan-2-aminium chloridum (**2d**) (colorless solid) m.p. = 230–231 °C (methanol); ^{1}H NMR ($CDCl_3$) δ = 1.79 (d, J_{HH} = 7.1 Hz, 3H, $CHCH_3$), 2.43 (s, 3H, CH_3), 2.85 (bs, 3H, NCH_3), 4.94 (bs, 1H, $CHCH_3$), 7.30 (d, J_{HH} = 8.0 Hz, 2H, aromatic), 7.84 (d, J_{HH} = 8.1 Hz, 2H, aromatic), 9.32 (m, 1H, NH_2), 10.51 (m, 1H, NH_2); ^{13}C{^{1}H} NMR ($CDCl_3$) δ = 16.49, 21.78, 31.72, 59.33, 129.00, 129.90, 130.58, 146.05, 194.25; IR (KBr): 3356 (νNH), 2964, 2910 (νPhH), 2803, 2741, 2722 (νCH_3), 1687 (νC=O), 1606 (scissor. NH_2), 1572 (νC=C), 1456 (νPhH), 1358, 1248 (νC-N), 756, 734 (wag. NH_2); UV–Vis (methanol; [nm]) (logε): 259.0 (5.20), 211.0 (5.02); X-ray CCDC 822035.

2-(Methylamino)-1-phenylbutan-1-one (**1e**) (yellowish liquid) ^{1}H NMR ($CDCl_3$) δ = 0.84 (dt, J_{HH} = 7.4 Hz, J_{HH} = 1.3 Hz, 3H, CH_2CH_3), 1.49 ($ABMX_3$, dqd, J_{HH} = 14.1 Hz, J_{HH} = 7.4 Hz, J_{HH} = 5.2 Hz, 1H, CH_2CH_3), 1.73 ($ABMX_3$, dqd, J_{HH} = 14.1 Hz, J_{HH} = 7.4 Hz, J_{HH} = 5.2 Hz, 1H, CH_2CH_3), 2.07 (bs, 1H, NH), 2.29 (s, 3H, $NHCH_3$), 4.01 (dd, J_{HH} = 6.5 Hz, J_{HH} = 5.3 Hz, 1H, $CHCH_2$), 7.40 (bt, J_{HH} = 7.5 Hz, 2H, aromatic), 7.49 (tt, J_{HH} = 7.4 Hz, J_{HH} = 1.3 Hz, 1H, aromatic), 7.89 (dd, J_{HH} = 8.3 Hz, J_{HH} = 1.2 Hz, 2H, aromatic); ^{13}C{^{1}H} NMR ($CDCl_3$) δ = 9.76, 26.39, 34.79, 65.07, 127.92, 128.52, 133.01, 136.19, 203.02.

N-Methyl-1-oxo-1-phenylbutan-2-aminium chloridum (**2e**) (colorless solid) m.p. = 190–191 °C (methanol); ^{1}H NMR ($CDCl_3$) δ = 1.02 (t, J_{HH} = 7.6 Hz, 3H, CH_2CH_3), 2.18 (dqd, J_{HH} = 15.0 Hz, J_{HH} = 7.5 Hz, J_{HH} = 5.1 Hz, 1H, CH_2CH_3), 2.39 ($ABMX_3$, dqd, J_{HH} = 15.0 Hz, J_{HH} = 7.5 Hz, J_{HH} = 5.1 Hz, 1H, CH_2CH_3), 2.85 (s, 3H, NH_2CH_3), 5.04 (t, J_{HH} = 5.2 Hz, 1H, $CHCH_2$), 7.52 (t, J_{HH} = 7.7 Hz, 2H, aromatic), 7.65 (t, J_{HH} = 7.4 Hz, 1H, aromatic), 7.98 (d, J_{HH} = 7.3 Hz, 2H, aromatic), 9.91 (m, 2H, NH_2CH_3); ^{13}C{^{1}H} NMR ($CDCl_3$) δ = 8.98, 23.71, 32.21, 63.98, 128.77, 129.19, 134.14, 134.70, 194.60.

2.2. DFT calculations

The calculations were carried out by using Gaussian09 [10] program. The DFT/B3LYP [11,12] method was used for the geometry optimization and electronic structure determination. The geometry optimizations were made for gas phase molecules. The calculations were performed using the polarization functions for all atoms: 6-31G** – carbon, nitrogen, oxygen and hydrogen. The contribution of a group to a molecular orbital was calculated using Mulliken population analysis. GaussSum 2.2 [13] was used to calculate group contributions (aromatic, *N*-aliphatic, $CH_3CHC(=O)$ fragments) to the molecular orbitals and to prepare the density of states (DOS). The DOS spectra were created by convoluting the molecular orbital information with Gaussian curves of unit height and Full Width at Half Maximum (FWHM) of 0.3 eV. The electrostatic potential (ESP) surfaces were plotted by using gOpenMol v2.31 program. The electronic spectra were calculated by the time-dependent density functional (TDDFT) [14] method based on the optimized geometries in the singlet states.

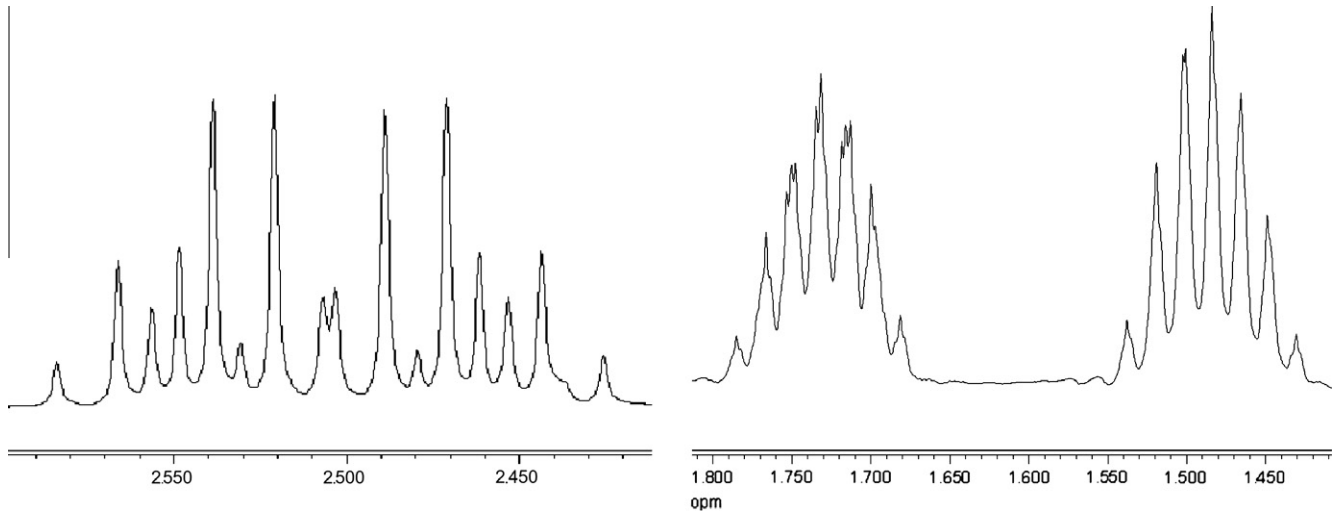

Fig. 1. The experimental ^{1}H NMR spectra in $CDCl_3$ of **1a** (left), **1e** (right); diastereotopic CH_2 protons regions.

Table 1a
The ^{1}H and ^{13}C chemical shifts of selected groups in $CDCl_3$.

		C=O	N—H	C—H	Aryl	R	R′
1a	^{1}H	–	2.22	4.29	2.41, 7.27, 7.86	1.29	1.10, 2.56
2a	^{1}H	–	9.02	4.96–5.06	2.43, 7.31, 7.86	1.81	1.53, 3.06–3.27
1b	^{1}H	–	–	4.05	5.97, 6.79, 7.38, 7.51	1.21	2.27
2b	^{1}H	–	–	4.76	6.11, 6.92, 7.42, 7.53	1.80	2.80
1c	^{1}H	–	1.93	4.10	2.21, 2.22, 7.12, 7.61, 7.66	1.19	2.26
2c	^{1}H	–	9.92	4.95	2.30, 2.32, 7.24, 7.67, 7.72	1.78	2.84
1d	^{1}H	–	2.26	4.14	2.30, 7.21, 7.80	1.23	2.34
2d	^{1}H	–	9.32, 10.51	4.94	2.43, 7.30, 7.84	1.79	2.85
1e	^{1}H	–	2.07	4.01	7.40, 7.49, 7.89	0.84, 1.49, 1.73	2.29
2e	^{1}H	–	9.91	5.04	7.52, 7.65, 7.98	1.02, 2.18, 2.39	2.85
1a	^{13}C	203.22	–	57.51	21.63, 128.33, 129.42, 133.10, 144.21	20.07	15.44, 42.35
2a	^{13}C	194.25	–	57.83	21.80, 128.96, 129.89, 130.44, 146.05	16.86	11.79, 42.12
1b	^{13}C	201.24	–	59.15	101.78, 107.90, 107.92, 124.32, 130.36, 148.22, 151.88	34.50	19.79
2b	^{13}C[a]	203.81	–	46.11	111.99, 117.42, 118.04, 135.32, 136.97, 157.71, 162.18	40.13	25.26
1c	^{13}C	202.85	–	59.05	19.58, 19.70, 125.65, 129.03, 129.65, 133.40, 136.82, 142.58	19.47	34.40
2c	^{13}C	194.43	–	59.25	19.77, 20.21, 126.54, 129.88, 130.32, 130.78, 137.71, 144.74	31.64	16.48
1d	^{13}C	202.68	–	59.21	21.55, 128.25, 129.35, 133.01, 144.17	19.64	34.47
2d	^{13}C	194.25	–	59.33	21.78, 129.00, 129.90, 130.58, 146.05	16.49	31.72
1e	^{13}C	203.02	–	65.07	127.92, 128.52, 133.01, 136.19	9.76, 26.39	34.79
2e	^{13}C	194.60	–	63.98	128.77, 129.19, 134.14, 134.70	8.98, 23.71	32.21

[a] In DMSO-*d6*.

Table 1b
The calculated ^{1}H and ^{13}C NMR chemical shifts of **1** and **2** in $CDCl_3$.

		C=O	N—H	C—H	Aryl	R	R′
1a	^{1}H	–	1.82	5.06	2.42, 7.26, 7.93	1.46	1.13, 2.83
2a	^{1}H	–	3.93	5.75	2.41, 7.41, 7.95	1.62	1.50, 3.22
1b	^{1}H	–	1.38	4.94	6.00, 6.75, 7.36, 7.62	1.52	2.37
2b	^{1}H	–	3.93	5.65	6.00, 6.85, 7.52, 7.62	1.62	2.71
1c	^{1}H	–	1.38	4.96	2.28, 2.52, 7.29, 7.53, 7.78	1.52	2.37
2c	^{1}H	–	3.93	5.67	2.20, 2.52, 7.39, 7.71, 7.92	1.62	2.71
1d	^{1}H	–	1.38	4.97	2.42, 7.26, 7.93	1.53	2.37
2d	^{1}H	–	3.93	5.67	2.41, 7.41, 7.95	1.62	2.71
1e	^{1}H	–	1.38	5.03	7.46, 7.49, 8.02	0.70, 1.43, 1.62	2.34
2e	^{1}H	–	3.93	4.92	7.50, 7.51, 8.17	0.97, 2.05	2.73
1a	^{13}C	202.19	–	47.91	21.66, 127.92, 129.44, 135.25, 144.10	15.40	14.80, 39.77
2a	^{13}C	205.84	–	52.06	21.67, 127.88, 128.73, 130.68, 145.46	10.96	9.03, 40.80
1b	^{13}C	200.03	–	49.74	102.11, 107.19, 108.93, 124.48, 130.21, 148.32, 150.05	32.20	15.33
2b	^{13}C[a]	192.60	–	42.51	101.47, 106.54, 108.12, 122.91, 125.71, 147.04, 152.01	6.89	30.75
1c	13C	202.31	–	49.05	19.65, 20.51, 127.77, 128.97, 130.20, 134.56, 139.00, 140.07	14.65	31.91
2c	^{13}C	205.96	–	45.56	19.99, 20.51, 127.23, 128.37, 129.15, 130.72, 137.95, 141.37	9.42	31.47
1d	^{13}C	201.90	–	49.19	21.66, 127.90, 129.44, 135.39, 144.10	14.78	31.91
2d	^{13}C	205.55	–	53.24	21.67, 127.88, 128.71, 130.82, 145.46	9.55	31.47
1e	^{13}C	202.16	–	56.83	127.96, 128.65, 132.98, 136.73	9.55, 24.37	33.33
2e	^{13}C	204.98	–	60.71	127.00, 128.20, 132.16, 133.74	10.60, 20.94	31.76

[a] In DMSO-*d6*.

2.3. Crystal structure determination and refinement

The colorless crystals of **2a**, **2b** and **2d** were mounted in turn on an Xcalibur, Atlas, Gemini ultra Oxford Diffraction automatic diffractometer equipped with a CCD detector for data collection. X-ray intensity data were collected with graphite monochromated Mo Kα radiation (λ = 0.71073 Å) at temperature of 295.0(2) K, with ω scan mode. Ewald sphere reflections were collected up to 2θ = 50.10. The unit cell parameters were determined from least-squares refinement at the setting angles of 3822, 5356, 2122 and 1830 strongest reflections for compounds **2a**, **2b**, **2c** and **2d**, respectively. Details of crystal data and refinement are gathered in Table 2. During the data reduction, the decay of the correction coefficient was taken into account. Lorentz, polarization, and numerical absorption corrections were applied. The structures were solved by direct method. All the non-hydrogen atoms were refined anisotropically using full-matrix, least-squares technique on F^2. All the hydrogen atoms were found from the difference of the Fourier synthesis after four cycles of anisotropic refinement, and refined as "riding" on the adjacent atom with individual isotropic temperature factor equal to 1.2 times the value of equivalent temperature factor of the parent atom, with geometry idealization after each cycle. The Olex2 [15] and SHELXS97, SHELXL97 [16] programs were used for all the calculations. Atomic scattering factors were those incorporated in the computer programs.

3. Results and discussion

The cathinones **1a**, **1b**, **1c**, **1d**, **1e** and their aminium salts **2a**, **2b**, **2c**, **2d**, **2e** were chosen as model compounds, and were characterized by multinuclear NMR spectroscopy, FTIR, UV–Vis, X-ray crystal structure analysis and computational studies. The information provided should be useful not only in the area of medical or pharmaceutical applications, but also in forensic or doping interest.

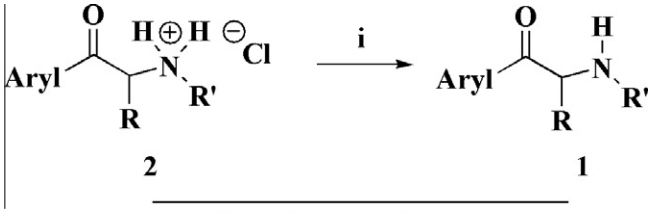

	R	R'	Aryl
a	Me	Et	4-MePh
b	Me	Me	1,3-benzodioxol
c	Me	Me	3,4-diMePh
d	Me	Me	4-MePh
e	Et	Me	Ph

Scheme 1. Chemical formulas of examined compounds. Reagents and conditions: i; K_2CO_3 20 °C.

3.1. NMR studies

The ^{1}H NMR solution spectra showed distinctive H-1 signals from CH, R or *N*-R′ groups. The diastereotopic methylene protons of **1a** appear as an ABX_3, and **1e** and **2e** appear as an $ABMX_3$ system (Fig. 1). Analysis of the trend in ^{1}H chemical shifts revealed that the deprotonation of nitrogen significantly increased the shielding effects, resulting the decreased chemical shifts of selected H-1 signals from CH, R or *N*-R′ groups. This corresponds well with the electrostatic potential (ESP) surfaces of cationic and neutral compounds (Fig. 4). The protonation of nitrogen for molecules **2** (or deprotonation for **1**) has the largest influence on C=O in C-13 spectroscopy (Tables 1a and 1b). The chemical shifts were moved to downfield (larger δ) for neutral molecules. The experimental and the calculated data are in good agreement (Tables 1a and 1b, Scheme 1).

Table 2
Selected details of the experimental diffraction data collections and refinements.

	2a	2b	2c	2d
Empirical formula	$C_{12}H_{18}NO$, Cl	$C_{11}H_{14}NO_3$, Cl	$C_{12}H_{18}NO$, Cl	$C_{11}H_{16}NO$, Cl
Formula weight	227.72	243.68	227.72	213.69
Temperature (K)	295.0(2) K	295.0(2) K	295.0(2) K	295.0(2) K
Crystal system	Monoclinic	Monoclinic	Orthorhombic	Monoclinic
Space group	$P2_1/c$	$P2_1/c$	*Pbca*	$P2_1/n$
Crystal color and shape	Colorless plate	Colorless plate	Colorless plate	Colorless plate
Unit cell dimensions				
a (Å)	7.2754(5)	11.1281(8)	12.6875(7)	7.1349(7)
b (Å)	14.9833(10)	23.2573(15)	9.0512(6)	23.031(4)
c (Å)	23.865(2)	10.3751(7)	21.9132(15)	7.4265(9)
β	93.423(7)	115.454(9)	90	90.477(11)
V (Å^3)	2596.9(3)	2424.5(3)	2516.5(3)	1220.3(3)
Z	8	8	8	4
Calculated density (Mg/m^3)	1.165	1.335	1.202	1.158
Mo Kα λ (Å)	0.71073	0.71073	0.71073	0.71073
Absorption coefficient (mm^{-1})	0.271	0.307	0.280	0.284
F(0 0 0)	976	1024	976	452
Crystal dimensions (mm)	0.32 × 0.17 × 0.06	0.30 × 0.28 × 0.18	0.39 × 0.24 × 0.05	0.43 × 0.14 × 0.11
θ range for data collection (°)	3.42–25.05	3.46–25.04	3.71–25.05	3.82–25.04
Index ranges	$-8 \leqslant h \leqslant 8$ $-17 \leqslant k \leqslant 17$ $-28 \leqslant l \leqslant 28$	$-13 \leqslant h \leqslant 13$ $-27 \leqslant k \leqslant 27$ $-12 \leqslant l \leqslant 12$	$-15 \leqslant h \leqslant 14$ $-9 \leqslant k \leqslant 10$ $-26 \leqslant l \leqslant 25$	$-6 \leqslant h \leqslant 8$ $-27 \leqslant k \leqslant 25$ $-8 \leqslant l \leqslant 8$
Reflections collected	19,243	18,318	8697	5447
Independent reflections	4583 [R_{int} = 0.0801]	4284 [R_{int} = 0.0304]	2227 [R_{int} = 0.0303]	1867 [R_{int} = 0.0253]
Data/restraints/parameters	4583/0/277	4284/0/293	2227/0/140	1867/0/130
Goodness-of-fit on F^2	1.025	1.031	1.032	1.096
Final *R* indices [$I > 2\sigma(I)$]	R_1 = 0.0400 wR_2 = 0.0910	R_1 = 0.0372 wR_2 = 0.0882	R_1 = 0.0388 wR_2 = 0.1023	R_1 = 0.0512 wR_2 = 0.0985
R indices (all data)	R_1 = 0.0675 wR_2 = 0.0998	R_1 = 0.0515 wR_2 = 0.0940	R_1 = 0.0569 wR_2 = 0.1103	R_1 = 0.0787 wR_2 = 0.0993
Largest diff. peak and hole (e Å^{-3})	1.036 and −0.684	0.189 and −0.216	0.227 and −0.165	0.463 and −0.293
CCDC number	823158	819333	822797	822035

3.2. IR studies

Infrared spectra of the compounds are close to each other and present characteristic bands due to the moiety of studied molecules. On the Fig. 2 the IR spectrum of compound **2b** is presented. The stretching modes of the free and hydrogen bonded NH present broad bands with the maximum at about 3350 cm^{-1}. The wagging modes of the amine are presented at 767 and 741 cm^{-1}, respectively. The carbonyl groups are indicated by the strong bands at 1679 cm^{-1}, in which the scissoring modes of NH_2 are expected. In the case of compound **2b** the ν_{C-O-C} frequencies of stretching and bending have the maximum at 1248 and 1187 cm^{-1}, respectively. The ν_{C-N} modes are observed in the range of 1358–1298 cm^{-1}. The band with maximum at 2449 cm^{-1} is attributed to combination band of the bending and libration modes of water molecules in crystal lattice. The IR transition was not calculated because the calculations were made for the gas phase.

3.3. X-ray studies

The hydrochloride salts **2a**, **2b** and **2d** crystallize in monoclinic ($P2_1/c$, $P2_1/n$) and the **2c** in the orthorhombic *Pbca* space groups.

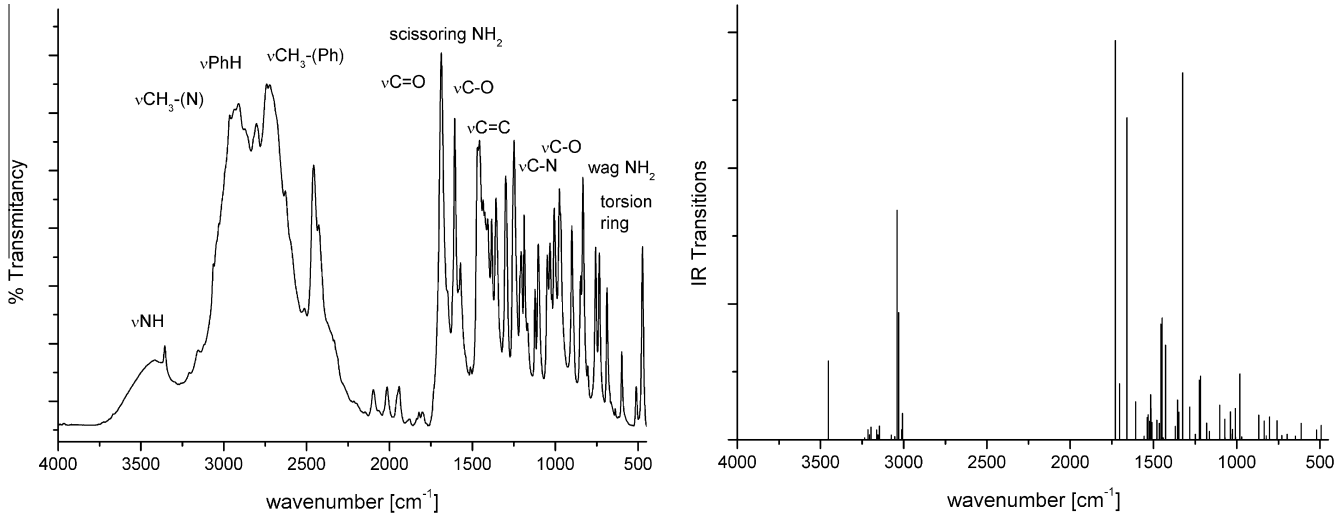

Fig. 2. Infrared spectrum of **2b** in KBr pellet; the experimental (left) and the calculated (right).

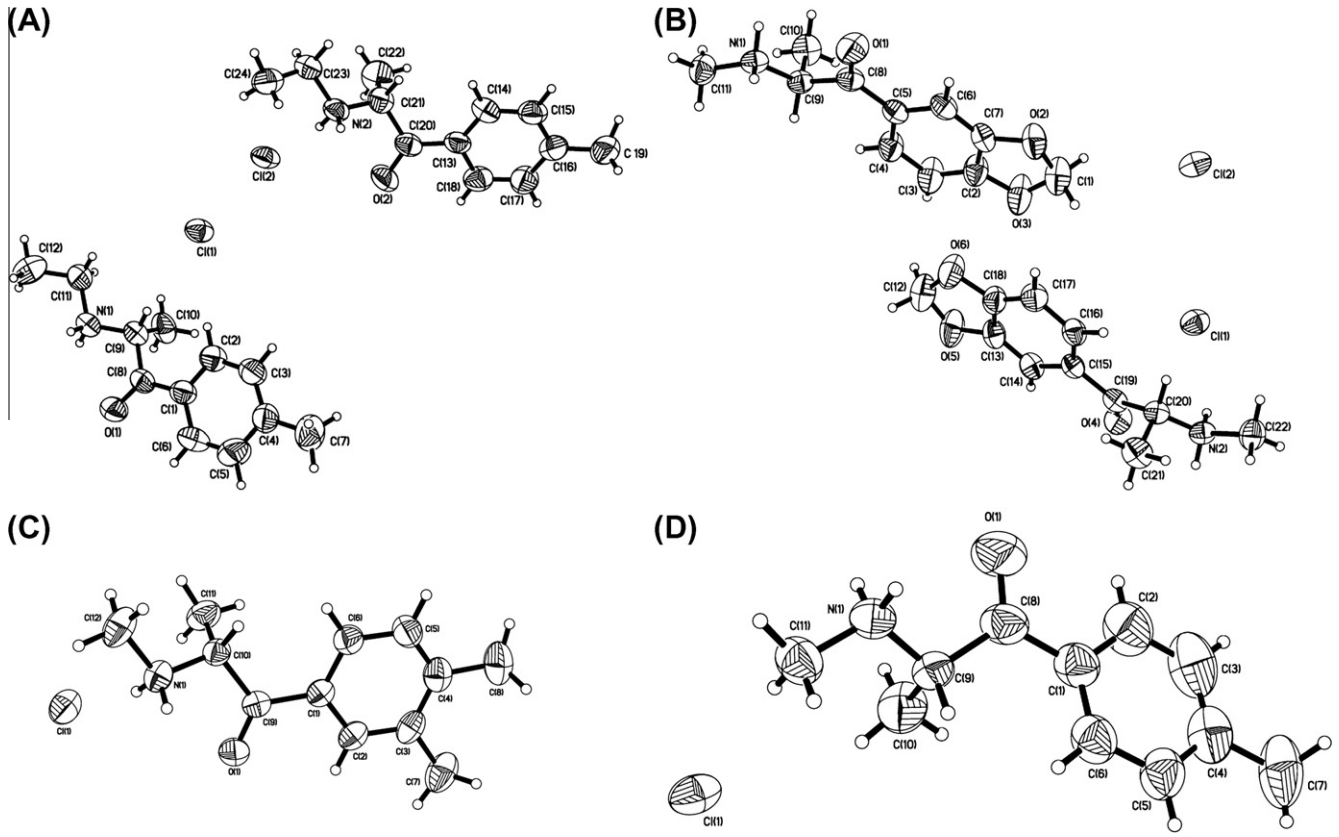

Fig. 3. ORTEP drawing of **2a**, **2b**, **2c** and **2d** molecules with 50% probability displacement ellipsoids.

Details of the crystal data and refinement are gathered in Table 2. The molecular structures of the studied compounds are shown in Fig. 3.

The molecular structures of compounds **2a** and **2b** are built up of two independent molecules in an asymmetric unit, in which the molecular ring systems in both studied compounds are essentially planar. All distances and angles (Table 3) in the molecular structures of the studied compounds are normal.

In the crystal structures of compounds **2a**, **2b** and **2c** sets of weak intermolecular hydrogen bonds are observed, and in the structure of **2d** one short intramolecular interaction can be considered as weak hydrogen bond. The cell packing of **2b** is presented on the Fig. 4 and one can see that no π-stacking interactions form in the crystal structure of the compounds.

3.4. Optimized geometries

To gain insight into the electronic structures and bonding properties of these complexes, DFT calculations were carried out. Before the calculations of electronic structures of the compounds, their geometries were optimized in singlet states using the B3LYP functional. From the data collected in Table 3, one may see that the

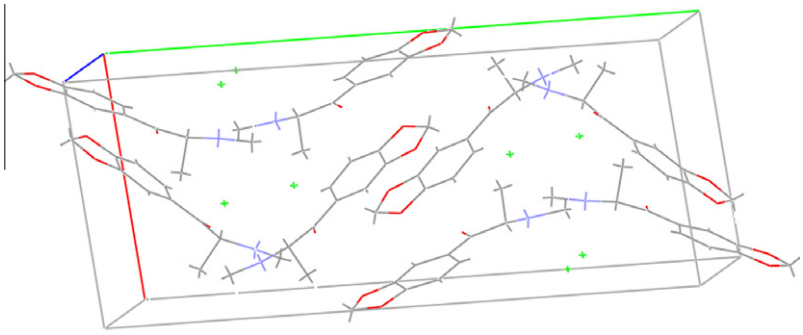

Fig. 4. The cell packing of **2b** compounds.

Table 3
Selected bond lengths and angles for compounds **2a**, **2b**, **2c** and **2d** with hydrogen bonds (Å and °).

	Bond lengths (Å)							
	2a		**2b**		**2c**		**2d**	
	Exp.[a]	Calc.	Exp.[a]	Calc.	Exp.	Calc.	Exp.	Calc.
C═O	1.214(14)	1.232	1.214(2)	1.235	1.216(2)	1.233	1.229(5)	1.233
N(1)—C(H)	1.464(14)	1.510	1.481(2)	1.496	1.479(2)	1.501	1.475(6)	1.497
N(1)—C($H_{2/3}$)	1.505(15)	1.520	1.486(2)	1.525	1.484(2)	1.515	1.477(5)	1.525
C_{aryl}—C═O	1.457(16)	1.457	1.476(3)	1.454	1.481(3)	1.459	1.486(7)	1.461
O═C—C	1.525(16)	1.559	1.519(3)	1.559	1.513(2)	1.559	1.507(6)	1.558
C—$C_{(alkyl)}$	1.526(16)	1.533	1.522(3)	1.531	1.525(3)	1.531	1.515(7)	1.532

Hydrogen bonds				
D—H···A	d(D—H)	d(H···A)	d(D···A)	∠(DHA)
2a				
N(1)—H(1A)···Cl(2) #1	0.90	2.22	3.082(9)	161.5
N(1)—H(1B)···Cl(1) #2	0.90	2.26	3.140(9)	167.3
N(2)—H(2A)···Cl(1) #3	0.90	2.23	3.097(9)	162.4
N(2)—H(2B)···Cl(2)	0.90	2.28	3.166(8)	166.1
C(9)—H(9)···Cl(1)	0.98	2.82	3.669(11)	146.0
C(15)—H(15)···O(2) #3	0.93	2.47	3.328(14)	153.6
C(21)—H(21)···Cl(2) #3	0.98	2.77	3.621(11)	145.4
2b				
N(1)—H(1A)—Cl(2) #4	0.90	2.22	3.0917(16)	164.0
N(1)—H(1B)—Cl(1) #4	0.90	2.21	3.0940(15)	166.7
N(2)—H(2A)—Cl(2) #2	0.90	2.32	3.1336(15)	149.6
C(3)—H(3)···O(3) #4	0.97	2.51	3.329(3)	141.9
C(15)—H(15C)···Cl(2) #5	0.93	2.47	3.368(3)	162.2
C(9)—H(9)···Cl(2) #6	0.98	2.75	3.6784(19)	157.7
C(12)—H(12A)···Cl(1) #7	0.97	2.82	3.770(3)	167.9
C(16)—H(16)···Cl(1)	0.93	2.79	3.717(2)	174.6
C(20)—H(20)···Cl(1)	0.98	2.65	3.5434(18)	151.7
2c				
N(1)—H(1A)—Cl(1) #8	0.90	2.25	3.1181(16)	162.7
N(1)—H(1B)—Cl(1)	0.90	2.25	3.1191(16)	162.3
C(10)—H(10)···O(1) #8	0.98	2.48	3.396(2)	155.9
2d				
N(1)—H(1A)—O(1)	0.90	2.53	2.656(5)	87.9

Symmetry transformations used to generate equivalent atoms: #1: 1 − *x*, 1/2 + *y*, 1/2 − *z*; #2: 1 + *x*, *y*, *z*; #3: −1 + *x*, *y*, *z*; #4: −*x*, −*y*, 1 − *z*; #5: −*x*, −*y*, −*z*; #6 −*x*, −1/2 + *y*, 1/2 − *z*; #7 1 − *x*, −*y*, −*z*; #8 3/2 − *x*, −1/2 + *y*, *z*.

[a] Average value.

bond lengths results from experiment and calculation are in reasonable agreement in the calculated gas phase structures. Fig. 2 shows that the calculated and experimental IR spectra of compound **2b** are in good agreement. Calculated IR spectra were used to analyze the experimental ones in Section 3.2.

The atomic charge calculations can give a feature for the relocation of the electron density of the compounds, but the local concentration and local depletion of electron charge density allow us to determine whether the nucleophile or electrophile can be attracted and allow understanding the mechanism of cathinones metabolism in humans and the side effects of metabolites. In Fig. 5, it only gives the plots of the electrostatic potentials for the studied compounds calculated for hydrochloride salt and hypothetical structures of neutral compounds. The Gibbons et al. predicted pK_a value for the methyl-cathinones as 8.4–9.5. They were most likely to be protonated at physiological pH [17]. The isoelectronic contours are plotted at 0.05 a.u. (31 kcal/mol). The color code of these maps is in the range between 0.05 a.u. (deepest red) to −0.005 a.u. (deepest blue) in all compounds, where blue indicates the strongest attraction and red indicates the strongest

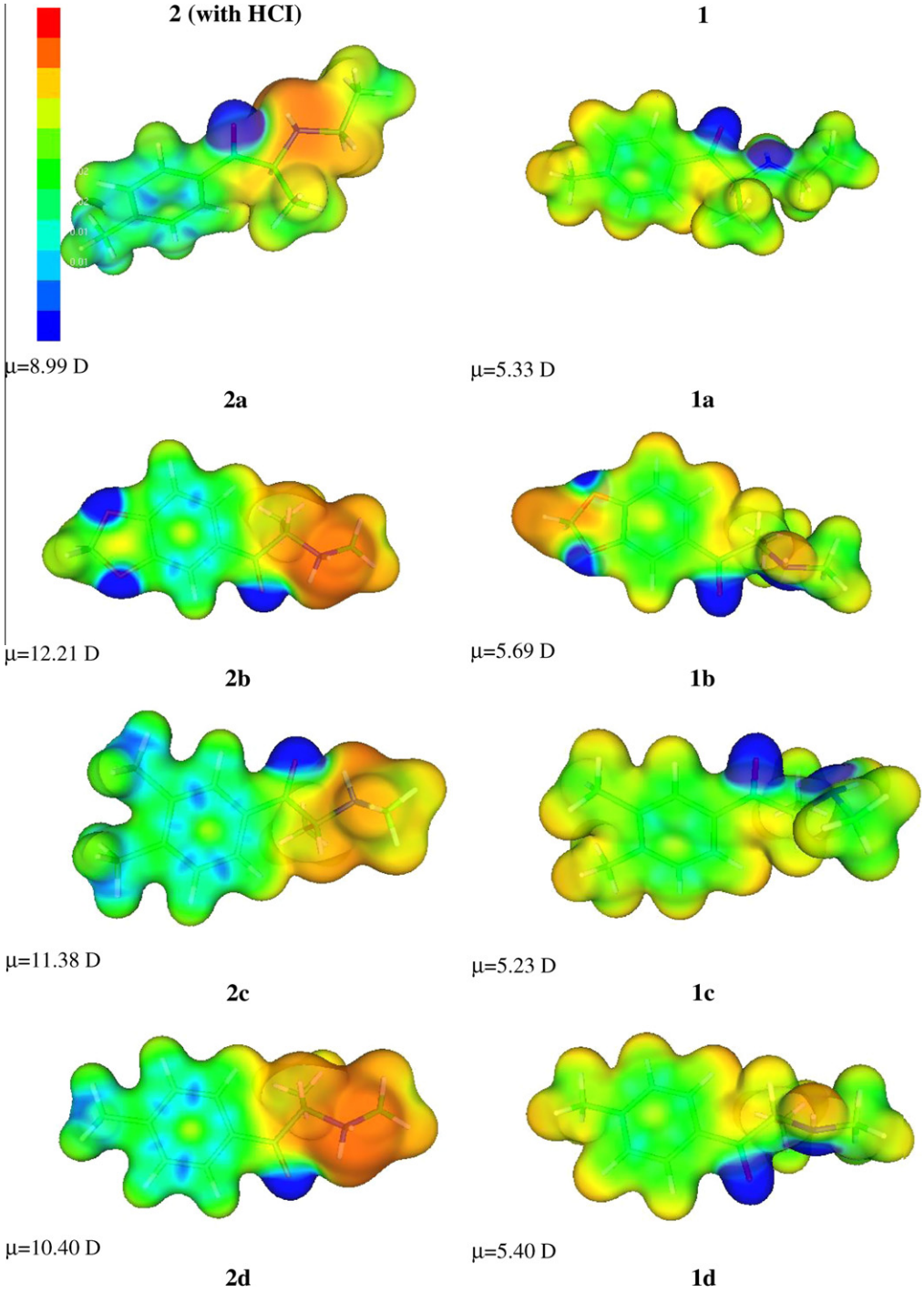

Fig. 5. Electrostatic potential (ESP) surfaces of cationic (left) and neutral (right) compounds. ESP surface is shown both in space (with positive and negative regions shown in blue and red, respectively) and mapped on electron densities (in the range of 0.05 a.u. – deepest red – to −0.005 a.u. – deepest blue) of the molecule (ESP color scale is chosen such that $\delta^+ \rightarrow \delta^-$ in the direction red → blue). (For interpretation of the references to color in this figure legend, the reader is referred to the web version of this article.)

repulsion. Regions of negative V(r) are usually associated with the lone pair of electronegative atoms.

The dipole moments of the compounds, calculated in methanolic solutions (PCM model), are presented in Fig. 5. As one can see the negative potentials are localized on the aryl part of the molecules of hydrochloric salt. Moreover the compound **2b** has the highest dipole moment and the maximum difference between the polarity of cationic and neutral forms (slightly higher than **2c**). In this manner we can consider that the polar electrodonating effects of CH_3 and 1,3-benzodioxolane groups are comparable.

3.5. Electronic structure

The electronic structures of the compounds are similar with each other. The partial density-of-states (DOS) in terms of Mulliken population analysis were calculated using the GaussSum program. They provide a pictorial representation of MOs compositions and their contributions to the chemical bonding. The PDOS diagrams are shown in Fig. 6. The PDOS plot mainly presents the composition of the fragment orbitals contributing to the molecular orbitals. The molecules of studied compounds were divided into the aromatic, *N*-aliphatic and $CH_3CHC(=O)$ fragments.

As one can see from the Fig. 6 in the frontier molecular orbitals of the compounds, the phenyl ring plays dominant role in HOMOs. In virtual MOs the amine part plays significant role. LUMOs are localized on the carbonyl and aryl moieties, while HOMOs are composed from phenyl π_2 and π_3 orbitals.

The HOMO–LUMO gaps vary between 4.47 eV for **2c** and 4.67 eV for **2a**, pointing the compounds as hard bases [18]. The compound **2b** is softer base with value of HOMO–LUMO gap 3.70 eV. The increase in energy levels of HOMO orbital in the **2b** compound is connected with the tune of π orbitals of 1,3-dioxol to the levels of benzene molecular orbitals.

The electronic spectra of the compounds are very similar. Fig. 7 presents experimental and calculated UV spectra of compound **2b**.

The calculations of electronic spectra were performed by using PCM model on the optimized structure at B3LYP/6-31G** level. The first experimental band with the maximum at 308 nm is connected with the HOMO → LUMO transitions (94%). In the bands with the maxima at 270 nm and 225 nm the transitions between H-1 → LUMO (81%; 11%) and HOMO → L + 1 (11%; 80%) were calculated. The highest energy band at 193 nm is contributed from the transitions between H-3 → LUMO (69%) and HOMO → L + 2 (24%). Taking into account the electronic structures of the compounds it is not surprised that the π-aromatic electrons are engaged into

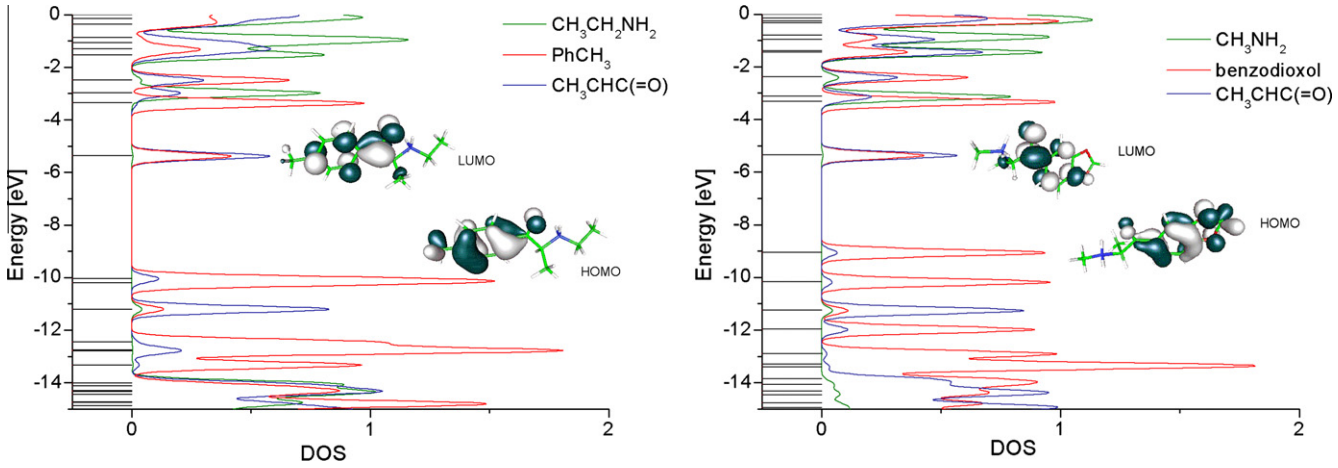

Fig. 6. The partial density of states (DOS) diagrams for compounds **2a** (left) and **2b** (right).

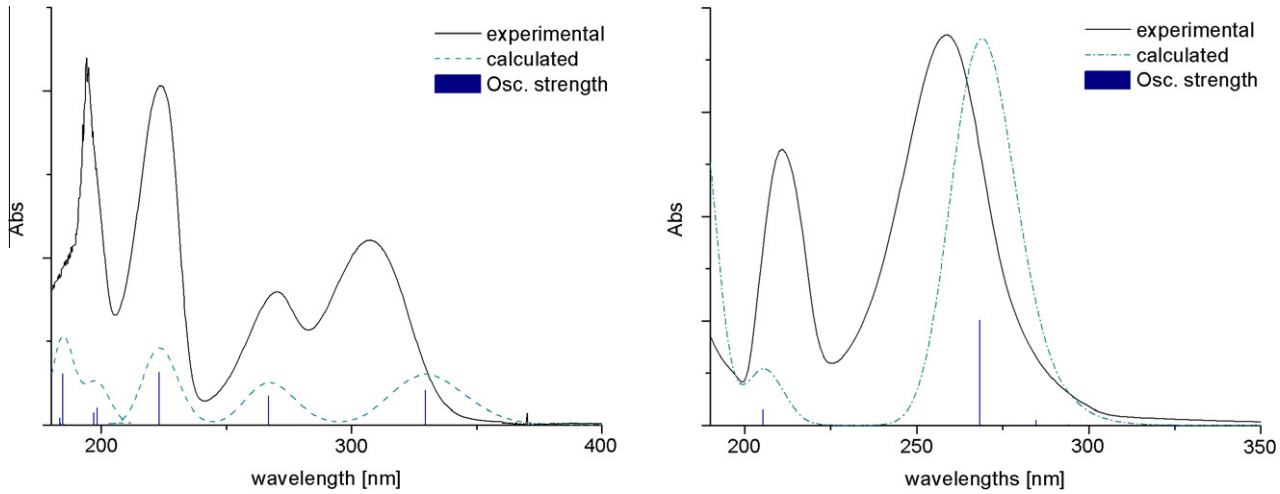

Fig. 7. Experimental and calculated electronic spectra of **2b** (left) and **2d** (right).

transitions. In the shortest wavelength, band transition from the carbonyl group is visible.

4. Conclusions

Further exploration in the structure of selected cathinones not only leads to the new applications of the compounds in the field of medicine or pharmaceuticals, but also is in the forensic or anti-doping interest. It also allows more understanding about the mechanism of cathinones metabolism in human body and the side effects of the metabolites. In general, the predicted bond lengths and angles fit well with the values obtained from the X-ray crystal structure. Similarly the calculated and experimental IR spectra of compound **2b** are in good agreement. The electronic structures of the compounds are similar with each other. NMR solution spectra showed characteristic H-1 and C-13 signals from CH, R, *N*-R (R = CH_3 or CH_2CH_3) or carbonyl groups. The diastereotopic methylene protons of **1a** appear as an ABX_3, and **1e** and **2e** appear as an $ABMX_3$ system.

5. Supplementary data

CCDC-823158 (for **2a**), 819333 (for **2b**), 822797 (for **2c**) and 822035 (for **2d**) contain the supplementary crystallographic data for the compounds. These data can be obtained free of charge from http://www.ccdc.cam.ac.uk/conts/retrieving.html, or from the Cambridge Crystallographic Data Centre, 12 Union Road, Cambridge CB2 1EZ, UK; fax: +44 1223 336 033; or e-mail: deposit@ccdc.cam.ac.uk. Calculations have been carried out in Wroclaw Centre for Networking and Supercomputing (http://www.wcss.wroc.pl).

The optimized geometrical parameters for compounds **2a**–**2d** are put as Supplementary data associated with this article.

Acknowledgments

We thank The Regional Headquarters Katowice for compound **2c**. The GAUSSIAN09 calculations were carried out in the Wrocław Centre for Networking and Supercomputing, WCSS, Wrocław, Poland (http://www.wcss.wroc.pl Grant Number 18).

References

[1] B.D. Berrang, A.H. Lewin, F.I. Carroll, J. Org. Chem. 47 (1982) 2643–2647.
[2] K.M. Prevatt-Smith, T.E. Prisinzano, Nat. Prod. Rep. 27 (2010) 23–31.
[3] P. Kalix, O. Braenden, Pharmacol. Rev. 37 (1985) 149–164.
[4] F. Schifano, A. Albanese, S. Fergus, J.L. Stair, P. Deluca, O. Corazza, Z. Davey, J. Corkery, H. Siemann, N. Scherbaum, M. Farre', M. Torrens, Z. Demetrovics, A.H. Ghodse, Psychopharmacology 214 (2011) 593–602.
[5] M.J.S. de Burnaga Sanchez, Bull. Soc. Chim. Fr. 45 (4) (1929) 284–286.
[6] R. Di Santo, R. Costi, A. Roux, M. Artico, O. Befani, T. Meninno, E. Agostinelli, P. Palmegiani, P. Turini, R. Cirilli, R. Ferretti, B. Gallinella, F. La Torre, J. Med. Chem. 48 (2005) 4220–4223.
[7] M.R. Meyer, J. Wilhelm, F.T. Peters, H.H. Maurer, Anal. Bioanal. Chem. 397 (2010) 1225–1233.
[8] K. Zaitsu, M. Katagi, H.T. Kamata, T. Kamata, N. Shima, A. Miki, H. Tsuchihashi, Y. Mori, Forensic Sci. Int. 188 (2009) 131–139.
[9] J.E. Nycz, G. Malecki, M. Zawiazalec, T. Pazdziorek, P. Skop, J. Mol. Struct. 984 (2010) 125–130.
[10] Gaussian 09, Revision A.1, M.J. Frisch, G.W. Trucks, H.B. Schlegel, G.E. Scuseria, M.A. Robb, J.R. Cheeseman, G. Scalmani, V. Barone, B. Mennucci, G. A. Petersson, H. Nakatsuji, M. Caricato, X. Li, H. P. Hratchian, A.F. Izmaylov, J. Bloino, G. Zheng, J.L. Sonnenberg, M. Hada, M. Ehara, K. Toyota, R. Fukuda, J. Hasegawa, M. Ishida, T. Nakajima, Y. Honda, O. Kitao, H. Nakai, T. Vreven, J.A. Montgomery, Jr., J.E. Peralta, F. Ogliaro, M. Bearpark, J.J. Heyd, E. Brothers, K.N. Kudin, V. N. Staroverov, R. Kobayashi, J. Normand, K. Raghavachari, A. Rendell, J. C. Burant, S.S. Iyengar, J. Tomasi, M. Cossi, N. Rega, J.M. Millam, M. Klene, J.E. Knox, J.B. Cross, V. Bakken, C. Adamo, J. Jaramillo, R. Gomperts, R.E. Stratmann, O. Yazyev, A.J. Austin, R. Cammi, C. Pomelli, J.W. Ochterski, R.L. Martin, K. Morokuma, V.G. Zakrzewski, G.A. Voth, P. Salvador, J.J. Dannenberg, S. Dapprich, A.D. Daniels, O. Farkas, J.B. Foresman, J.V. Ortiz, J. Cioslowski, D.J. Fox, Gaussian, Inc., Wallingford, CT, 2009.
[11] A.D. Becke, J. Chem. Phys. 98 (1993) 5648–5652.
[12] C. Lee, W. Yang, R.G. Parr, Phys. Rev. B 37 (1988) 785–789.
[13] N.M. O'Boyle, A.L. Tenderholt, K.M. Langner, J. Comp. Chem. 29 (2008) 839–845.
[14] M.E. Casida, in: J.M. Seminario (Ed.), Recent Developments and Applications of Modern Density Functional Theory, Theoretical and Computational Chemistry, vol. 4, Elsevier, Amsterdam, 1996, p. 391.
[15] O.V. Dolomanov, L.J. Bourhis, R.J. Gildea, J.A.K. Howard, H. Puschmann, J. Appl. Cryst. 42 (2009) 339–341.
[16] G.M. Sheldrick, Acta Cryst. A64 (2008) 112–122.
[17] S. Gibbons, M. Zloh, Bioorg. Med. Chem. Lett. 20 (2010) 4135–4139.
[18] R.G. Pearson, Inorg. Chim. Acta 270 (1998) 252–260.